Energy & Environmental Science

PAPER

View Article Online
View Journal

Check for updates

Cite this: DOI: 10.1039/c9ee00626e

3D hierarchical porous amidoxime fibers speed up uranium extraction from seawater†

Xiao Xu,[ab] Hongjun Zhang,[c] Junxuan Ao,[ad] Lu Xu,[a] Xiyan Liu,[a] Xiaojing Guo,[e] Jingye Li,[a] Lan Zhang,[a] Qingnuan Li,[a] Xiaoyan Zhao,[b] Bangjiao Ye,[c] Deli Wang,[f] Fei Shen[dg] and Hongjuan Ma*[a]

Received 25th February 2019,
Accepted 25th April 2019

DOI: 10.1039/c9ee00626e

rsc.li/ees

The development of amidoxime-based polymeric (ABP) fibers offers a solution for uranium extraction from seawater (UES) and provides an alternative solution to the uranium resource shortage. However, ABP adsorbents prepared by existing methods cannot meet the requirements of high adsorption capacity, high selectivity, good mechanical strength and long service life. Herein, we fabricated a 3D hierarchical porous, high specific surface area ABP (H-ABP) fiber *via* self-assembly of axial grafting chains. A high adsorption capacity of 11.50 mg-U per g-adsorbents was achieved in natural seawater, which is a significant breakthrough in UES. Meanwhile, the adsorption capacity of uranium was higher than its major competing element vanadium, which overturned the U/V mass ratio of the ABP fiber. The H-ABP fiber also exhibited good mechanical strength and a long service life of at least 10 adsorption–desorption cycles. The well-designed structure resulted in groundbreaking properties, which completely meet the requirements for the economic evaluation of UES. This work presents a new technology for the synthesis of highly efficient adsorbents for UES, thus opening a whole new means of nuclear fuel production from the ocean.

Broader context

The 4.5 billion tons of uranium in seawater, which is 1000 times larger than the amount of uranium in terrestrial ores, is considered a powerful guarantee for rapid development of nuclear technologies. Adsorbents prepared by existing methods cannot meet requirements of economic evaluation of uranium extraction from seawater (UES), *i.e.*, a disposable adsorbent with a 30 mg-U per g-adsorbents capacity or a service life of 10 adsorption–desorption cycles with a 6 mg-U per g-adsorbents and average 3% capacity loss per cycle. Here we report a fundamental breakthrough in demonstrating 3D hierarchical porous, high specific surface area ABP (H-ABP) fibers *via* self-assembly of axial grafting chains by two step polymerization. The properties of high adsorption capacity (11.50 mg-U per g-adsorbents) in natural seawater, a mechanical strength of 131.10 MPa, a service life of at least 10 adsorption–desorption cycles and high selectivity of uranium from this H-ABP fiber enable the final uranium production cost of UES be \$170–206 per kg-uranium, which is close to the criteria for the economic evaluation of adsorbents. This advancement in adsorbent synthesis will have a transformative effect on the industrialization process of UES and industrial production of uranium from the ocean takes a major step forwards.

Given its special use in the nuclear industry, uranium has become more of an economic resource than a natural resource. With the development of nuclear technologies, the discrepancy between production and demand for uranium has become increasingly apparent.[1,2] Because of the large amount of uranium in the ocean, seawater has been considered an important unconventional uranium source.[3,4] Compared with mining, uranium extraction from seawater (UES) is more environmentally friendly; however, it faces enormous challenges, including the extremely low uranium concentration of 3.3 ppb that primarily presents in the form of uranyl tricarbonate, and a large amount of competing ions.[5,6] In view of this, UES is considered as one of the seven chemical separations to change the world.[7]

[a] Shanghai Institute of Applied Physics, Chinese Academy of Sciences, Shanghai 201800, China. E-mail: mahongjuan@sinap.ac.cn
[b] School of Petrochemical Engineering, Changzhou University, Changzhou 213164, China
[c] State Key Laboratory of Particle Detection and Electronics, University of Science and Technology of China, Hefei 230026, China
[d] University of Chinese Academy of Sciences, Beijing 100049, China
[e] The Department of Chemistry and Chemical Engineering, Shanghai Normal University, Shanghai 200234, China
[f] State Key Laboratory of Marine Environmental Science, Xiamen University, Xiamen 361005, China
[g] Institute of Process Engineering, Chinese Academy of Sciences, Beijing 100190, China

† Electronic supplementary information (ESI) available. See DOI: 10.1039/c9ee00626e

After more than half a century of research on UES, the use of amidoxime (AO)-based polymeric (ABP) fibers has been recognized as the most promising approach.[7–9] In the early 2000s, researchers from the Japan Atomic Energy Agency (JAEA) successfully captured 1 kg of uranium yellow cake with ABP adsorbents prepared by radiation-induced grafting polymerization (RIGP).[10] However, the ABP fiber used at that time displayed a limited adsorption capacity of 1.5 mg of uranium per g of adsorbents (mg-U per g-adsorbents) over 30 days of exposure in seawater.[11] In order to increase the specific surface area of the adsorbents, a hollow ABP fiber was synthesized at the Oak Ridge National Laboratory (ORNL), which showed an adsorption capacity of 4.50 mg-U per g-adsorbents in seawater.[12–14] They also reported another type of ABP fiber prepared by atom-transfer radical polymerization (ATRP) with a capacity of 5.22 mg-U per g-adsorbents in seawater.[15] Recently, a fully amidoximated nanofiber,[16] a porous amidoxime-based nanofiber,[17] a biomass-derived microporous membrane[18] and an electrochemical method[19] have also been developed for UES. Amidoximated nanofiber synthesized by Wang *et al.* exhibited an 8.7 mg-U per g-adsorbents capacity in 0.22 μm filtered natural seawater after 56 days of adsorption, which was the highest capacity reported in the field of UES until now.[16,17] However, ABP adsorbents prepared by existing methods cannot meet requirements of economic evaluation, *i.e.*, a disposable adsorbent with a 30 mg-U per g-adsorbents capacity or a service life of 10 adsorption–desorption cycles with 6 mg-U per g-adsorbents and average 3% capacity loss per cycle.[20–22] The industrialization of UES crucially depends on the properties and cost of the required materials. Despite the availability of these materials and new techniques, their adsorption capacities and selectivity cannot meet the requirements for disposability, and their mechanical strengths do not enable long service life. Based on the findings of previous research, making fibers hollow or reducing their diameter to nanometers will indeed increase the specific surface area of adsorbents, but will simultaneously decrease their mechanical strengths. Commercial trunk polymeric fibers, such as polyethylene (PE) and polypropylene (PP) with diameters of 10–20 μm, generally exhibit breaking strengths of hundreds of MPa and thus have much greater mechanical strength than hollow fibers or nanofibers. It would be better to increase the specific surface area of the grafted layer rather than that of the trunk material.

Here we first report a novel technology to fabricate a 3D hierarchical porous, high specific surface area ABP (H-ABP) fiber *via* self-assembly of axial grafting chains. This new method maintains the mechanical strength of the trunk fiber while increasing the specific surface area of the grafted layer, which results in a material with long service life and remarkable adsorption performance. The H-ABP fibers were fabricated using a two-step graft polymerization involving the RIGP of 2-hydroxyethyl acrylate (HEA) onto a commercial PE-coated PP skin-core (PE/PP) fiber followed by the Ce^{4+} initiated graft polymerization (CIGP) of acrylonitrile (AN) and acrylic acid (AA) onto the poly-HEA (PHEA) chains. The microstructure, tension, service life and adsorption behavior of the fiber were investigated in both simulated seawater and natural seawater. A high adsorption capacity of 11.50 mg-U per g-adsorbents was achieved after 90 days of adsorption in natural seawater, which is the highest reported in the literature. Furthermore, the adsorption capacity of uranium was higher than its major competing element vanadium, which overturned the U/V mass ratio of the ABP fiber due to the 3D hierarchical porous structure. This H-ABP fiber also exhibited good mechanical strength and a long service life of at least 10 adsorption–desorption cycles. The high adsorption capacity, high selectivity over vanadium, excellent reusability, good mechanical strength, structural stability and relatively low manufacturing costs suggest that the H-ABP fiber already meets the requirements for the economic evaluation of UES.

The schematic diagram in Fig. 1a and b illustrates the preparation of the H-ABP fiber using a two-step graft polymerization (RIGP–CIGP). The durable H-ABP fiber was synthesized as follows: (1) RIGP of HEA onto a commercial trunk PE/PP fiber at a very low absorbed dose (10 kGy) to provide the hydroxyl group (–OH) as a reducing agent, and (2) CIGP of AN and AA using ceric ammonium nitrate/nitric acid (CAN/HNO_3) as a strong oxidant. The mechanism and schematic of CIGP are shown in Fig. S1 (ESI†). Finally, H-ABP fibers were obtained with amidoximation of the fibers above. In the previous study, to introduce a sufficient quantity of nitrile groups on the trunk fiber, traditional RIGP of AN and AA was carried out at a high absorbed dose of 80–200 kGy,[23,24] which obviously resulted in higher costs and damage to the substrate fiber. Furthermore, the inability to tune the morphology of the grafted layer from the RIGP restricted the material properties.[16,22,25] CIGP of AN and AA on specific sites of side chains gave birth to axial grafting chains along the trunk fibers rather than radial direction grafting chains from RIGP, which resulted in a well-designed structure certainly and remarkable adsorption performance (Fig. 1b and c).

RIGP of HEA and CIGP of AA and AN were systematically studied to investigate the optimal grafting conditions (Fig. S2, ESI†). PHEA with a 15% degree of grafting (DG) was denoted as PE/PP-*g*-PHEA. After CIGP, the DG of poly-AA-*co*-poly-AN (PAA-*co*-PAN) was 110% and this was denoted as PE/PP-*g*-PHEA-(PAA-*co*-PAN). After amidoximation, the representative AO group density of the resulting H-ABP fiber was 5.1 mmol g^{-1} (eqn (S3), ESI†).

The grafting and chemical modification of the PE/PP fiber were studied by Fourier transform infrared spectrometry (FT-IR) and X-ray photoelectron spectroscopy (XPS). The characteristic adsorption bands from FT-IR spectra at 2914 and 2847 cm^{-1} of trunk PE/PP fibers (Fig. S3, trace a, ESI†) were attributed to the asymmetric and symmetric stretching of the $-CH_2-$ groups on the fiber. Compared with the PE/PP-*g*-PHEA spectra (Fig. S3, trace b, ESI†), the adsorbance intensity of –C═O– (1724 cm^{-1}) in the PE/PP-*g*-PHEA-(PAA-*co*-PAN) spectra (Fig. S3, trace c, ESI†) was significantly increased and the new stretching vibrations of –C≡N occurred at 2247 cm^{-1}, indicating that HEA, AA and AN were all successfully grafted onto the trunk PE/PP fibers.[12] The disappearance of the nitrile stretch at 2247 cm^{-1} coupled with the appearance of $-NH_2$/–OH (3100–3500 cm^{-1}), –C═N– (1642 cm^{-1}), C–N (1381 cm^{-1}) and N–O (916 cm^{-1}) in H-ABP fibers (Fig. S3, trace d, ESI†) verified the conversion of nitrile groups to amidoxime groups. On the XPS spectra,

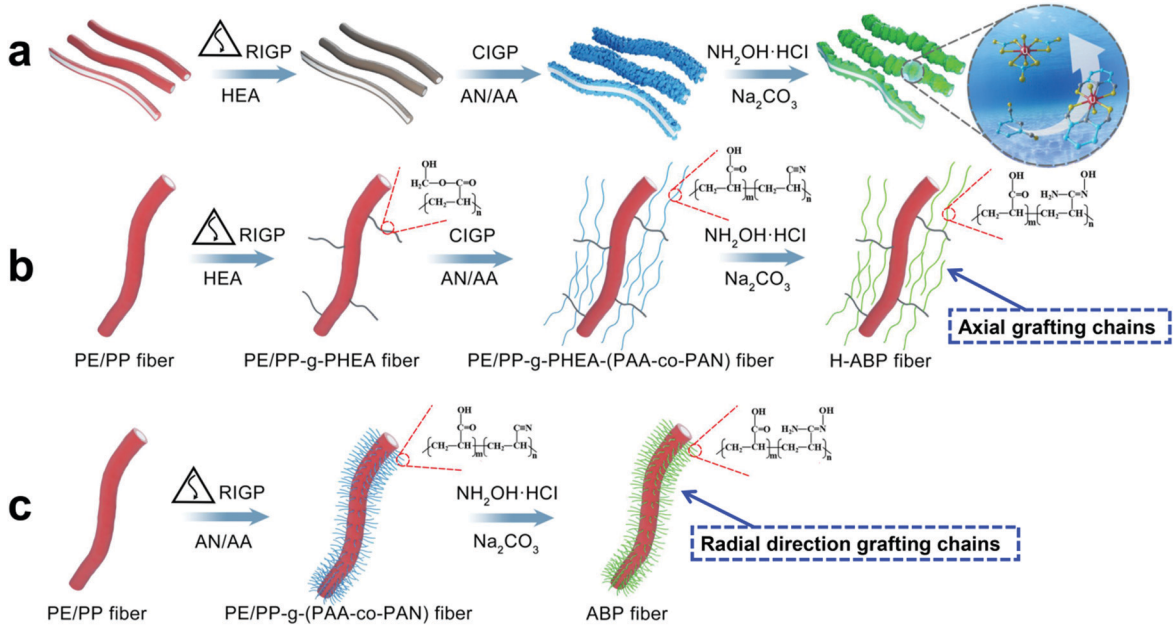

Fig. 1 Schematic diagram of the preparation of H-ABP fiber. (a) Preparation of a controllable order morphology with a 3D hierarchical porous structure and functional polymer particle H-ABP fiber. (b) Structural evolution of grafted chains in H-ABP fiber induced by RIGP and CIGP. (c) Structural evolution of grafted chains in the ABP fiber induced by RIGP.

compared with the PE/PP fiber, PE/PP-*g*-PHEA fibers showed a new peak at 531.8 eV (O 1s) indicating the successful grafting of PHEA onto the surface of the trunk PE/PP fibers (Fig. S4a, ESI†). Following graft modification, the N 1s (399.6 eV) peak appeared on the XPS survey scan for PE/PP-*g*-PHEA-(PAA-*co*-PAN) fibers and H-ABP fibers (Fig. S4a, ESI†). The C 1s peak of H-ABP fibers shown in Fig. S4b (ESI†) consists of four peaks that corresponded to C–C, C–O/N, C═N and O═C–O groups. The N 1s spectrum of H-ABP fibers in Fig. S4c (ESI†) has three emerging peaks, which were attributed to N–H, C═N and N–O groups. The O 1s spectrum of H-ABP fibers in Fig. S4d (ESI†) has three emerging peaks, which were attributed to C–O, N–O and C═O species, further illustrating that the H-ABP fiber was successfully synthesized.[16]

CIGP of AN and AA onto specific sites of side chains gave birth to axial grafting chains along the trunk fibers rather than radial direction grafting chains that result from RIGP (Fig. 1b and c). This process is highly controllable and a high specific surface area fiber with functional polymer particles and a 3D hierarchical porous structure was finally obtained *via* self-assembly of axial grafting chains (Fig. 2).

The morphology of the trunk and H-ABP fibers was characterized by scanning electron microscope (SEM) and transmission electron

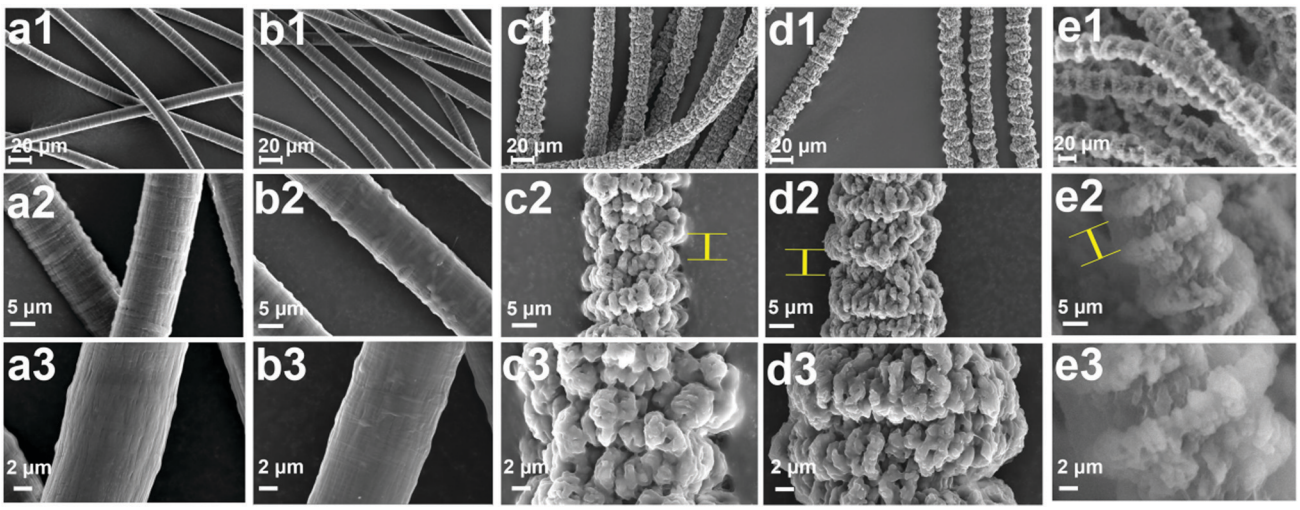

Fig. 2 Surface morphology characterization. SEM images of PE/PP, PE/PP-*g*-PHEA, PE/PP-*g*-PHEA-(PAA-*co*-PAN) and H-ABP fiber at different magnifications (a1–3), (b1–3), (c1–3), and (d1–3). Environmental scanning electron microscopy (ESEM) image of the H-ABP fiber obtained in a wet state after soaking the H-ABP fiber with deionized water for three days (e1–3).

microscope (TEM). Trunk PE/PP fibers showed an average diameter of 12.5 ± 0.2 μm (Fig. 2a1–a3). The relatively low DG (15%) of PHEA resulted in a relatively smooth morphology and a diameter for the PE/PP-*g*-PHEA fiber similar to that of the trunk PE/PP fiber (Fig. 2b1–b3). After CIGP with AA and AN, the average diameter of the resulting PE/PP-*g*-PHEA-(PAA-*co*-PAN) fibers increased markedly. Self-assembly of axial grafting chains of AN and AA resulted in functional polymer particles and a 3D hierarchical porous structure in the fiber (Fig. 2c1–c3). Following amidoximation, a novel, well-designed, H-ABP fiber with functional polymer particles and a 3D hierarchical porous structure was constructed (Fig. 2d1–d3). Cross sections of the PE/PP fibers showed a PP core layer and a PE skin layer (Fig. 3a). The H-ABP fibers are composed of a PP core layer, a PE skin layer and an outward growing grafted polymer layer shown in the TEM images (Fig. 3b). Uniform functional polymer particles on the grafted polymer layer showed an average polymer particle size of about 500 nm. Importantly, this morphology can be very well retained in water (Fig. 2e1–e3).

This ordered morphology with functional polymer particles and a 3D hierarchical porous structure exhibited high specific surface area. The roughness was determined using an atomic force microscope (AFM). The root mean square (Rq) roughness of the PE/PP trunk fibers was 58.4 nm as shown in Fig. S5a (ESI†), and in comparison, the roughness for H-ABP fibers greatly increased to 271.0 nm as shown in Fig. S5b (ESI†). N_2 sorption isotherms and pore diameter distribution curves of H-ABP fiber, ABP fiber and trunk PE/PP fiber are shown in Fig. 3c and Fig. S6 (ESI†). The Brunauer–Emmett–Teller (BET) surface area of H-ABP was 12.7 $m^2\ g^{-1}$, which is nearly three times that of the trunk PE/PP fiber (4.3 $m^2\ g^{-1}$) and ten times that of the hollow gear morphology ABP fiber (1.35 $m^2\ g^{-1}$).[12] Meanwhile, H-ABP fibers showed a hierarchical porous structure with a total pore volume (0.0074 $cm^3\ g^{-1}$) greater than that of the trunk PE/PP fiber (0.0014 $cm^3\ g^{-1}$). This preparation process could be regulated to control the polymer conformation and resulting morphology by changing the DG of the PE/PP-*g*-PHEA fiber, which represents the number of active sites for CIGP (Fig. S7, ESI†). Then DG of PE/PP-*g*-PHEA-(PAA-*co*-PAN) was controlled to obtain an appropriate amount of functional polymer particles. Thus, optimizing the grafting process and following specific surface area of the fiber adsorbent would greatly improve the adsorption performance for UES.

The effects of the DG of the PE/PP-*g*-PHEA-(PAA-*co*-PAN) fibers on the BET surface area of the H-ABP fibers are shown in Fig. S8a (ESI†). The BET surface area of the H-ABP fibers increased with increasing DG up to 110%, which corresponded to the highest BET surface area of 12.7 $m^2\ g^{-1}$. This could be attributed to the Ce^{4+}-induced polymerization and ammoximation into a highly 3D hierarchical porosity. However, with futher increase in the DG, the BET surface area slowly decreased. Tightly-bound accumulation between the polymer particles reduced the 3D hierarchical porosity of the H-ABP fibers. In Fig. S8b (ESI†), it is shown that the effect of the uranium adsorption capacity of H-ABP fibers on the DG of PE/PP-*g*-PHEA-(PAA-*co*-PAN) fibers is the same as that of the corresponding BET surface area. The adsorption capacity increased to 5.73 mg-U per g-adsorbents with increasing

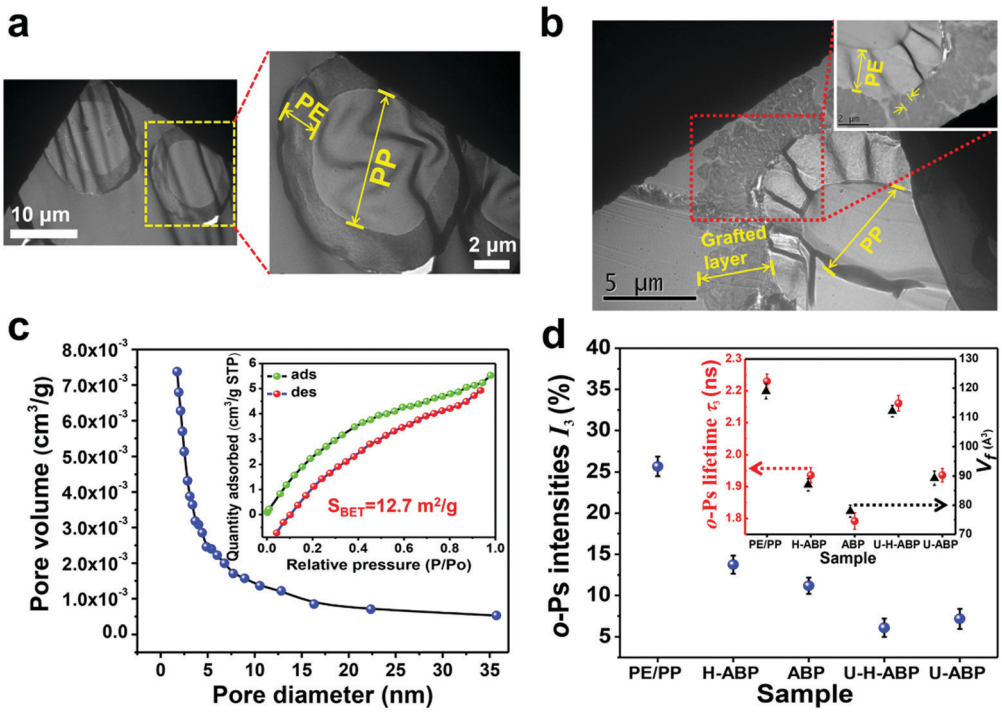

Fig. 3 3D hierarchical porous structural characterization. TEM images of the (a) PE/PP and (b) H-ABP fiber cross section and enlargement of the H-ABP fiber cross section. (c) Pore diameter distributions of the H-ABP fiber. Inset: N_2 sorption isotherms of the H-ABP fiber. (d) The *o*-Ps intensities from PE/PP, H-ABP, ABP, U-H-ABP, and U-ABP fibers. Inset shows the *o*-Ps lifetime (left-*Y*-axis, red symbols) and V_f (right-*Y*-axis, black symbols) of free-volume holes from PE/PP, H-ABP, ABP, U-H-ABP, and U-ABP fibers.

DG and then decreased. This suggests that the reduction in the 3D hierarchical porosity hinders the diffusion of seawater and uranium into the inner part of the fiber, and significantly reduces the utilization efficiency of AO ligands. Accordingly, a DG of 100–150% provides an appropriate density and utilization percentage of functional groups in the application of uranium adsorption.

Positron annihilation lifetime (PAL) spectroscopy is a unique experimental technique used to characterize the nanometer-scaled free-volume holes in polymers.[26] The *ortho*-positronium (*o*-Ps) lifetime is determined by the size of the free-volume holes, and its intensity is closely correlated with the fraction of the free-volume holes. Using the LTv9 program, all PAL spectra were resolved into three lifetime components of τ_1, τ_2 and τ_3, with corresponding intensities of I_1, I_2 and I_3, respectively.[27] Among the three lifetime components, the longest component τ_3 corresponds to the *o*-Ps annihilation in free-volume holes. Using the Tao–Eldrup model, the average radius (R) of free-volume holes can be estimated from the *o*-Ps lifetime, τ_3:

$$\tau_3^{-1} = 2\left[1-\frac{R}{R+\Delta R}+\frac{1}{2\pi}\sin\left(2\pi\frac{R}{R+\Delta R}\right)\right] \quad (1)$$

where ΔR (0.1656 nm) is the thickness of the electron layer on the surface of the free-volume holes.[28,29] The average volume (V_f) of free-volume holes, which is usually called the free-volume hole size, can be estimated from the following equation:

$$V_f = 4\pi R^3/3 \quad (2)$$

As shown in Fig. 3d and the inset, *o*-Ps intensities and *o*-Ps lifetimes for H-ABP and ABP fibers decreased after grafting and chemical modification compared to the trunk PE/PP fibers. During the preparation process, RIGP of HEA onto trunk PE/PP fiber was carried out at an absorbed dose of 10 kGy, which is much lower than that of ABP fibers (80 kGy). Since the *o*-Ps lifetime is related to the hole size around *o*-Ps,[30] shortening of the *o*-Ps lifetime indicates densification of the polymer due to radiation-induced-crosslinking of PE in the skin layer of the trunk PE/PP fiber. Furthermore, grafting and amidoximation with the monomers HEA, AN, AA and NH_2OH all resulted in a decrease in *o*-Ps intensities and *o*-Ps lifetimes for the ABP fibers compared with the PE/PP fibers. As expected, the values of *o*-Ps intensities and *o*-Ps lifetimes for H-ABP were higher than those for the ABP fiber. This indicates that the H-ABP fibers have a more porous structure than the ABP fibers as observed both on the sub-nanometer scale by PAL spectroscopy and on the micrometer scale by SEM, ESEM, TEM and BET measurements.

After the subsequent uranium adsorption, U-ABP exhibited an *o*-Ps lifetime much longer than that of ABP fibers. Similarly, the *o*-Ps lifetime for U-H-ABP was also higher than that for H-ABP fibers. According to previous studies, the presence of metals and metal oxides in porous materials tends to diminish both *o*-Ps lifetime and *o*-Ps intensity, which is due to the inhibition of *o*-Ps formation and chemical quenching of *o*-Ps annihilation.[31] The increment in *o*-Ps lifetime after uranium adsorption is most probably caused by a sufficient occupancy of smaller free-volume holes and an insufficient occupancy of bigger free-volume holes. This clearly suggests that, for both ABP and H-ABP fibers, occupancy of uranium in smaller sub-nanometer scaled free-volume holes is easier than in larger free-volume holes in the fibers.

By contrast, the *o*-Ps intensity for U-H-ABP fibers was lower than that for U-ABP fibers. Since the *o*-Ps intensities can be related to the number of holes in the polymers.[26] For H-ABP fibers, uranium adsorption induced a decrement in the *o*-Ps intensity much bigger than that observed for ABP fibers. The decrease in the *o*-Ps intensity is due to the prohibition effect on *o*-Ps formation and the chemical reaction of *o*-Ps annihilation with metals and metal oxides.[31] Therefore, the bigger decrement of *o*-Ps intensity between U-H-ABP and H-ABP fibers indicates that, more uranium was adsorbed by the H-ABP fiber. These results provide additional evidence for the later discussion, and also explain why the adsorption performance of the H-ABP fiber was better than that of the ABP fiber.

The adsorption performance of the H-ABP fiber was investigated in the coastal marine areas of Guangdong, China. In this work, the average concentrations of uranium and competing ions in natural seawater are shown in Table S3 (ESI†). The color of the H-ABP fibers changed from white to yellow and gradually to dark brown in natural seawater (Fig. S9c and d, ESI†). The results of uranium adsorption from seawater are presented in Fig. 4a and Table S1 (ESI†). The uranium capacity increased almost linearly with increasing adsorption time over the duration of the first 60-day test. After 36 days of adsorption in natural seawater, the capacity was 5.40 mg-U per g-adsorbents, which is higher than the capacity that was reported for the ORNL's adsorbent (5.22 mg-U per g-adsorbents) after a period of 49 days with filtration.[15] The uranium capacity increased to 8.30 mg-U per g-adsorbents after 56 days of adsorption in natural seawater. After 90 days of adsorption, the adsorption capacity reached 11.50 mg-U per g-adsorbents, which is still far from saturation and is the highest reported in the literature. During the 90 days of adsorption, the H-ABP fiber showed good selectively of U over V, Fe, Ni, Cu, Zn, Pb and Co but not Ca and Mg as the concentrations of Ca and Mg were much higher than that of U (Table S3, ESI†). Ca and Mg do not pose a problem as they can be easily eluted with low concentrations of eluant. The adsorption capacities of V, Fe, Ni, Cu, Zn, Pb and Co using H-ABP fiber were 8.12, 3.86, 0.32, 0.47, 0.43, 0.05, and 0 mg per g-adsorbents, respectively, after 90 days of exposure. Impressively, the H-ABP fiber showed high U/V mass ratio of U over V. Contrarily, ABP fiber showed a low U/V mass ratio of U (3.61 mg-U per g-adsorbents) over V (4.97 mg-V per g-adsorbents) (Fig. S10 and Table S2, ESI†). In the UES field, the selectivity of U and V has been persued by researchers for years as ABP adsorbents generally show a higher capacity for V than U. What's more, V cannot be eluted completely from the adsorbents, even with high concentrations of eluant.[15,16,24] Impressively, the H-ABP fiber not only triggered the enhancement in uranium uptake capacity compared to the ABP fibers, but also overturned the U/V mass ratio.

Up to now, significant controversy exists over the precise coordination environment for U and V, specifically regarding

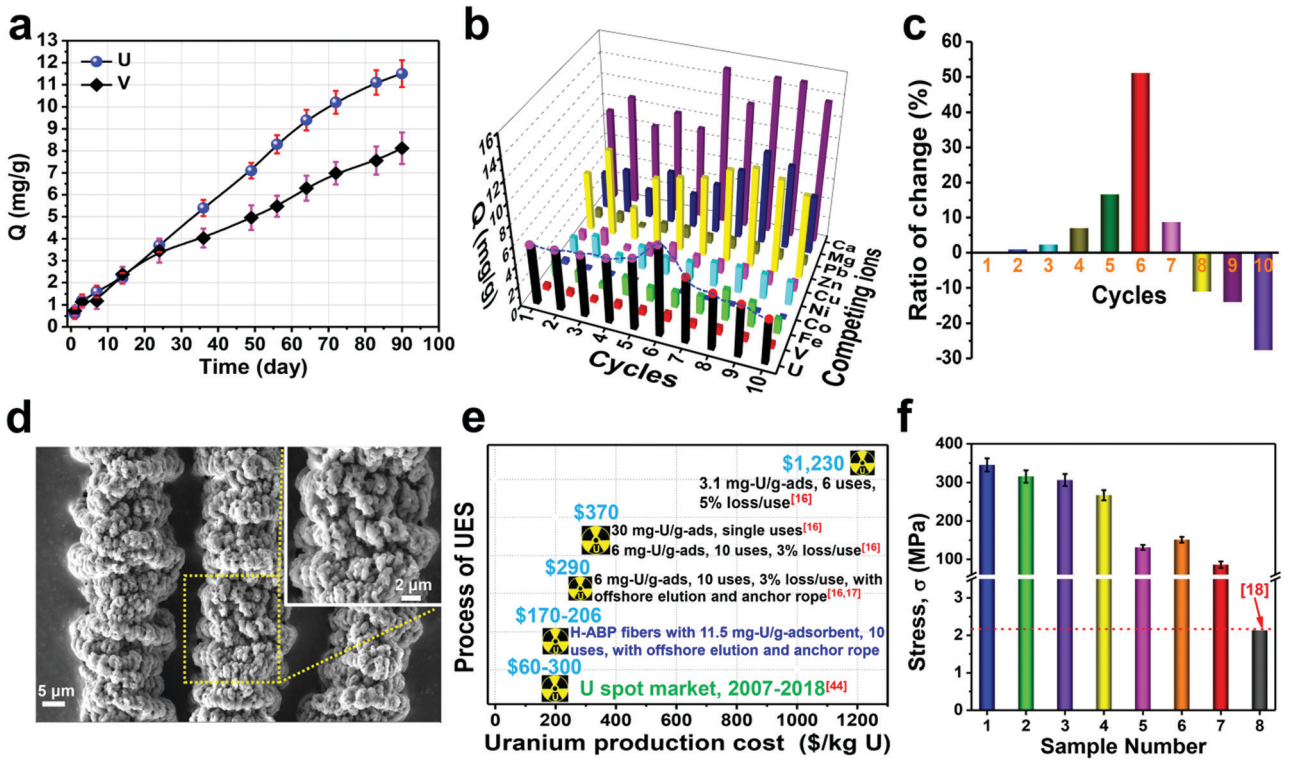

Fig. 4 Adsorption performance and reusability of H-ABP fiber. (a) Uranium and vanadium adsorption capacities of H-ABP fibers during different contact periods with natural seawater during the marine test. (b) Uranium adsorption capacity during the 10 adsorption–desorption cycles of H-ABP fibers in simulated seawater system B with an initial uranium concentration of 330 ppb and coexisting ions of V, Fe, Co, Ni, Cu, Zn, Pb, Mg, and Ca. (c) Ratio of change in uranium adsorption capacity during the 10 adsorption–desorption cycles of H-ABP fibers in simulated seawater system B relative to the first absorption cycle. (d) SEM images of H-ABP fiber after 10 adsorption–desorption cycles. The inset shows the order morphology with a 3D hierarchical porous structure and functional polymer particles of the H-ABP fiber after 10 adsorption–desorption cycles at a higher magnification. (e) UES production cost progression and H-ABP fiber is a milestone in the industrialization process of UES. (f) Breaking strength for single (1) PE/PP, (2) pre-irradiation of PE/PP fibers with 10 kGy, (3) PE/PP-*g*-PHEA, (4) PE/PP-*g*-PHEA-(PAA-*co*-PAN), (5) H-ABP, (6) H-ABP fiber in a wet state, (7) H-ABP fiber after 10 adsorption–desorption cycles in simulated seawater systerm B, and (8) nanofibers reported in the literature.

the open chain amidoxime functionalities *versus* the cyclic imide dioxime.[32–34] Many studies have shown that V binds preferentially with cyclic imide dioxime group and does not bind well with open chain amidoxime.[32,33] And XAFS investigations also suggest a lessened coordination role of the cyclic imide dioximes,[12] and no evidence to support the binding of U by cyclic imide dioximes.[34] The ^{13}C CP/MAS spectra of H-ABP and ABP fibers are illustrated in Fig. S11 (ESI†). The signals at 148.7 ppm and a shoulder centered at 157.1 ppm are ascribed to cyclic imide dioxime and open chain amidoxime of H-ABP fibers, respectively.[35,36] Furthermore, the signals at 178.6 ppm are ascribed to COO^- (*i.e.*, AA).[15] However, the ^{13}C CP/MAS spectra of ABP fibers show a slightly stronger signal at 149.8 ppm (Fig. S11, ESI†), and no shoulder centered at 157.1 ppm. The results indicated that H-ABP fibers might have less cyclic imide dioxime than ABP fibers, and more open chain amidoxime than ABP fibers, which might be one of the main reasons why the U/V mass ratio of H-ABP fibers is higher than that of ABP fibers. However, such subtle differences cannot overturn the U/V mass ratio from traditional ABP materials. We believe that it was not the structure of open chain amidoxime and the cyclic imide dioxime affects the U/V mass ratio from H-ABP fiber as both H-ABP fiber and ABP fiber contains these two functional groups. As temperature is important to the structure of AO: low temperature resulted in open chain amidoxime, while high temperature resulted in a cyclic imide dioxime group,[37,38] we studied the effect of reaction temperature of amidoximation on the adsorption performance and U/V mass ratio of H-ABP fibers. The results suggested that with the increase of amidoximation reaction temperature, the adsorption capacity for U and V (Fig. S12a, ESI†) as well as the AO density on the H-ABP fiber increased correspondingly (Fig. S12b, ESI†). However, the U/V mass ratio showed the opposite trend: even though U/V mass ratio decreased with increment of temperature, the U/V mass ratio tended to be stable at 1.91 when the temperature was higher than 55 °C (Fig. S12b, ESI†). The U/V mass ratio was always higher than 1 for H-ABP fiber under different amidoximation reaction temperatures in the range of 25–85 °C. The results show that the low reaction temperature of amidoximation is beneficial for the selective adsorption of U on H-ABP fibers, which was shown previously through small molecule studies.[37] However, the adsorption capacity is limited from the adsorbents prepared under lower amidoximation temperature. Hence, we prefer a high amidoximation reaction temperature of 70 °C. From this

point of view we suggest that the H-ABP fiber is a structure-based adsorbent where the adsorption capacity and selectivity are significantly affected by the polymer conformation but not the cyclic imide-dioxime or open-chain amidoxime.[34]

The low selectivity for U compared to V by the traditional ABP fiber is due in part to the random rotation of the functional molecular chains in an open chelating space that offers AO functional groups equal opportunity to contact the competing ions.[39] It is well known that the adsorption kinetics of U by ABP fiber are faster while binding is weaker compared to V.[40] The proposed factor affecting the selectivity would be the ordered morphology with a 3D hierarchical porous structure. Functional polymer particles on the surface of the H-ABP fiber can also serve as unique hosts for the capture of uranium. H-ABP fibers with 3D hierarchical porosity favor the free diffusion of seawater and uranium, thereby enhancing the adsorption kinetics of U.[41,42] After preferential binding of uranium, functional molecular chains in the 3D hierarchical porous structure lose their ability to freely rotate due to the pore confinement effect and consequently, V cannot easily take the place of U.[39]

Besides adsorption capacity and selectivity, the adsorbent's service life is a key factor requiring consideration in its industrial application as it greatly affects the cost of the UES. The adsorption capacity and stability of the H-ABP fiber were studied in two simulated seawater systems: first, simulated seawater system A, the same as ORNL's simulated seawater adsorption system where the initial concentration of uranium was 8 ppm.[12] The highest adsorption capacity exhibited by the hollow gear morphology AF 1 fiber under these conditions was 225 mg-U per g-adsorbents compared to 4.5 mg-U per g-adsorbents in natural seawater.[12] Fig. 5a shows the plot of the normalized uranium adsorption capacity against the number of repetitions of adsorption and elution from the H-ABP fiber. The H-ABP fiber showed a high adsorption capacity of 302 mg-U per g-adsorbents and no loss of capacity after five adsorption–desorption cycles. After that, the recycled H-ABP fibers exhibited a 4.1%, 13.4% and 19.3% loss in capacity at the sixth, seventh and eighth adsorption–desorption cycles, respectively, relative to the first adsorption. However, the adsorption capacity still remained high at 234 mg-U per g-adsorbents (Fig. 5a and Table S4, ESI†). Further reuse of the H-ABP fiber resulted in an obvious loss of adsorption capacity. The H-ABP fiber exhibited better adsorption capacity as well as longer service life than the AF1 fiber under the same conditions.

Given the low uranium concentration at the ppb level and the presence of competing ions in natural seawater, we implemented rapid screening of adsorbents within 24 h using simulated seawater system B (Table S3, ESI†). Fig. 4b shows the adsorption capacity of uranium and competing ions against the number of repetitions of adsorption and elution from the H-ABP fiber. The adsorption capacity of the H-ABP fiber was 5.73 mg-U per g-adsorbents in the first adsorption cycle. The H-ABP fiber showed good selectively of U over V, Fe, Co, Ni, Cu and Pb during the 10 adsorption–desorption cycles, which agrees very well with the results in natural seawater. Similar to the results in simulated seawater system A, the H-ABP

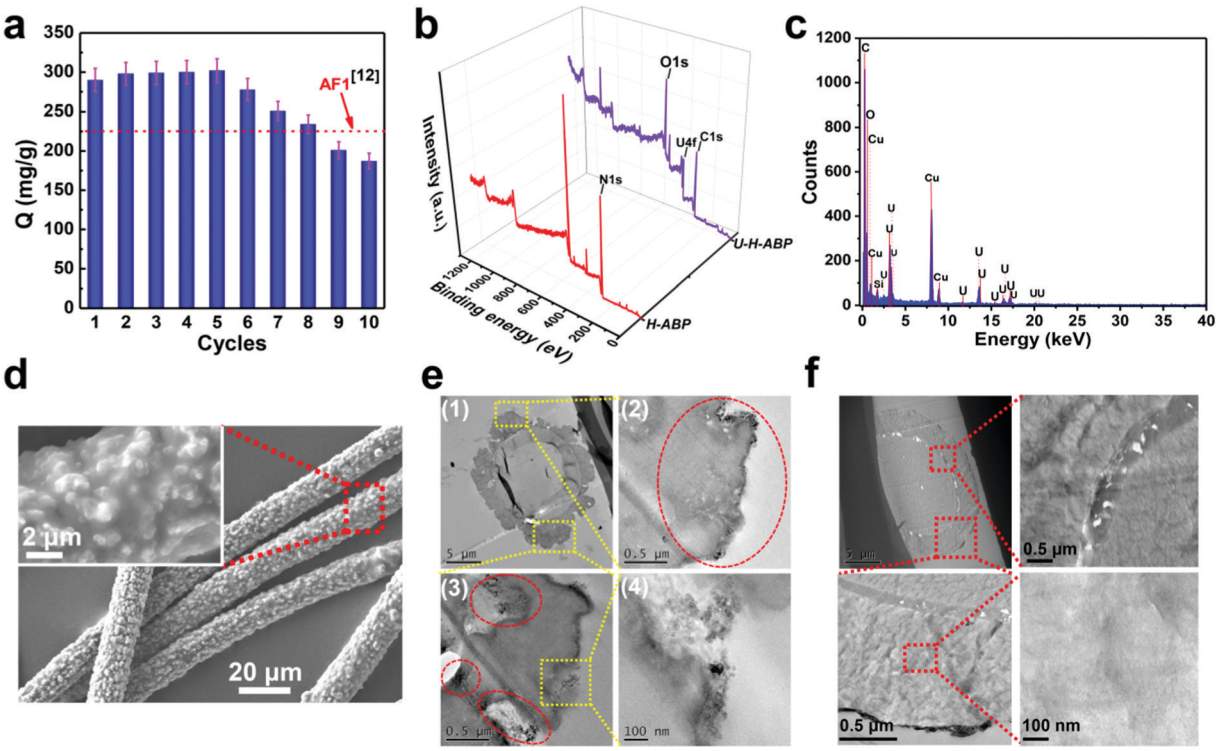

Fig. 5 Structure and morphology of U-H-ABP fiber. (a) Uranium adsorption capacity during the 10 adsorption–desorption cycles of H-ABP fibers in simulated seawater system A with an initial uranium concentration of 8 ppm. (b) The XPS spectra of H-ABP and U-H-ABP fiber, respectively. (c) The EDX spectroscopic analysis for the U-H-ABP fiber. (d) SEM image showing the morphology of the U-H-ABP fiber. TEM images of the (e) U-H-ABP and (f) U-ABP fiber cross section at different magnifications.

fiber showed no loss but rather an increase in uranium adsorption capacity. Compared with the first adsorption cycle, the H-ABP fibers exhibited a 0.9%, 2.3%, 7.0%, 16.6%, 51.1%, and 8.7% increase in uranium adsorption capacity after subsequent adsorption–desorption cycles, followed by a loss of 11.0%, 14.0% and 27.7% (Fig. 4c and Table S4, ESI†). The service life of the H-ABP fiber attained in this study is the best that has been reported in the literature.

Results from both simulated seawater system A and B suggest that H-ABP fiber exhibited a slight increment of uranium capacity during the first five adsorption–desorption cycles. There are two possible causes for this phenomenon: (1) the ordered morphology with a 3D hierarchical porous structure and functional polymer particles enabled the H-ABP fibers to swell after a period of time soaking in simulated seawater. In particular, the diameter of H-ABP fiber increased with the increase of adsorption–desorption cycles (Fig. S13a, ESI†), and the daimeter of H-ABP fiber increased almost 20.1% after 10 adsorption–desorption cycles (Fig. S13a and S14, ESI†). AFM analysis indicated that the Rq roughness of the wet state H-ABP fibers decreased to 136.0 nm from 271.0 nm of dry H-ABP fibers (Fig. S5c, ESI†). SEM images also showed a different surface morphology of the H-ABP fiber after 10 adsorption–desorption cycles (Fig. S14, ESI†). Gradual swelling of the grafted layer facilitated the penetration and diffusion of seawater and uranium to the inner part of the H-ABP fiber;[43] (2) after elution with HCl and regeneration with NaOH, functional polymer particles in the H-ABP fiber are gradually seperated into smaller polymer particles (Fig. S14, ESI†). The gaps between polymer particles also facilitated the penetration and diffusion of seawater and uranium to the inner part of the H-ABP fiber. However, after 5 or 6 adsorption–desorption cycles, the capacity of uranium decreased with the increase of the number of adsorption cycles. After 10 adsorption–desorption cycles, H-ABP fibers was digested with microwaves and the residual amount of U and competing ions is shown in Fig. S13b (ESI†). The results showed that almost no uranium remained in H-ABP fiber while the residual amounts of V and Fe were 1.02 mg g^{-1} and 1.51 mg g^{-1}, respectively. V and Fe residues still occupied AO ligands as their binding strengths are higher than that of U and were difficult to elute completely.[38,40] This is one of the reasons why ABP adsorbents lose their capacity after repeated use.

A disposable adsorbent with a 30 mg-U per g-adsorbents capacity or an adsorbent with a 6 mg-U per g-adsorbents adsorption capacity at 3% capacity loss per use with 10 uses (51.90 mg-U per g-adsorbents in total) would result in a price of $290 per kg-uranium, which is comparable to the price of uranium from conventional terrestrial resources ($100–335 per kg-uranium).[20–22] Based on the 10 cycle capacity summary shown in Table S4 (ESI†), the extraction capacity of the H-ABP fiber was 59.23 mg-U per g-adsorbents, which was higher than 51.90 mg-U per g-adsorbents. Given the prime capacity of 11.50 mg-U per g-adsorbents in natural seawater, there is reason to believe that the fabrication cost of H-ABP fibrous adsorbent would be reduced to about 50%. Chemicals used in the graft polymerization, washing, and amidoximation steps dominate the material costs, which represent about 58–83% of the UES total production cost.[20] Accordingly, without consideration of associated costs, the final cost of UES using an H-ABP fiber would be about $170–206 per kg-uranium, which is close to the criteria for the economic evaluation of adsorbents used for UES (Fig. 4e).[21,22,44]

The morphology of uranium loading onto H-ABP fiber was characterized by SEM and TEM. The SEM images showed a dense surface of H-ABP fibers after adsorption of 302 mg-U per g-adsorbents (Fig. 5d). The full scan XPS analysis of uranium loading in H-ABP fibers confirmed the presence of uranium, oxygen, carbon and nitrogen atoms on the adsorbent surface (Fig. 5b). From TEM images of the cross section of uranium loading on the H-ABP fiber, it can be seen that uranium covered the entire graft layer by adsorbing to the polymer particles on the surface of the H-ABP fiber as well as the inner 3D hierarchical porous structure (Fig. 5e(1–3)). The nano-scale TEM images in Fig. 5e(4) show ion clusters of uranium distributed over the surface and inner part of the H-ABP fiber. Multiple energy-dispersive X-ray analysis (EDX) mappings of these ion clusters and EDX analysis of uranium loading on H-ABP fibers indicated the presence of uranium distributed throughout the grafted layer (Fig. 5c). From TEM images of the cross section of uranium loading on the ABP fiber, no ion clusters of uranium were observed at the inner part of ABP fiber (Fig. 5f). The result indicated that the structure-based adsorbent (H-ABP fiber), *i.e.*, the polymer conformation, significantly influenced the adsorption capacity.[34]

The mechanical strength of a single fiber is important as each fiber should be able to withstand the force of the ocean current. The representative breaking strength and stress–strain curves are presented in Fig. 4f and Fig. S15a (ESI†), respectively. The breaking strength of the trunk PE/PP fiber was 345.01 ± 0.12 MPa (Fig. 4f(1)). During the synthesis process, an obvious decrease in mechanical strength of the fiber was noted with each step due to irradiation with RIGP and the following chemical grafting and modification. Even so, the resulting H-ABP fiber still maintained a mechanical strength of 131.10 ± 0.14 MPa (Fig. 4f(5)). The flexibility and strength of the PE/PP fiber were maintained as the initiation sites for AN and AA grafting were created on the PHEA molecular chain rather than the trunk PE/PP fiber. After 10 adsorption–desorption cycles, the mechanical strength was 86.02 ± 0.21 MPa (Fig. 4f(7)), which is much higher than 2.13 MPa from the nanofibers reported in the literature.[16] A bundle of H-ABP fibers (5 g, 1 m long) can withstand the weight of an adult, which illustrates the excellent mechanical strength of H-ABP fibers and suggests that they could be used in ocean currents (Fig. S15b and inset, ESI†). In addition to mechanical strength, high structural stability is also crucial for real applications in the ocean. The morphology of the H-ABP fibers after 10 adsorption–desorption cycles is shown in Fig. 4d inset and Fig. S14b (ESI†). The ordered morphology with functional polymer particles and a 3D hierarchical porous structure was well kept in highly saline water and was immune to elution and regeneration.

The innovative well-designed structure and simple synthesis approach make these adsorbents promising for practical applications. The significant enhancements in the uranium adsorption capacity, selectivity and service life of the H-ABP fiber are attributed to its novel morphological characteristics: (1) the specific surface

area of the H-ABP fiber was tremendously increased compared to that of the ABP fiber; (2) the ordered morphology with functional polymer particles and a 3D hierarchical porous structure attained *via* self-assembly from axial grafting chains accelerated the free diffusion of seawater and uranium into the fiber, and provided the grafting chain with enough space for swelling; and (3) the high structural stability of this ordered morphology in seawater consolidates the advantages of high specific area during uranium adsorption.

Conclusions

In summary, the innovative well-designed 3D hierarchical porous structure of the H-ABP fiber resulted in ground-breaking properties for UES. The simple synthesis approach makes these adsorbents promising for practical applications. The H-ABP fiber reaches meters in length, which allows it to settle easily in seawater like seaweed. H-ABP's uranium adsorption capacity of 11.50 mg-U per g-adsorbents, high U/V mass ratio, long service life of 10 adsorption–desorption cycles and good mechanical strength indicate that this fiber already meets the requirements for economic evaluation in the application of UES. The fabrication of this H-ABP fiber is a milestone in the industrialization process of UES, and industrial production of uranium from the ocean takes a major step forwards.

Author contributions

H. Ma had the idea of fabricating high specific surface area amidoxime-based polymeric fibers using two-step graft polymerization. X. Xu, H. Zhang, H. Ma, F. Shen and J. Li designed the experiments. X. Xu, H. Ma, J. AO, L. Xu, X. Liu, X. Guo and H. Zhang performed the experiments. X. Xu, J. Li, L. Zhang, Q. Li, B. Ye and D. Wang analysed the data, X. Xu and H. Ma co-wrote the paper. All authors discussed the results and commented on the manuscript.

Conflicts of interest

The ordered morphology with a 3D hierarchical porous structure and functional polymer particles of H-ABP fibers used for uranium adsorption has been filed as a patent application 201810409276.3 submitted by Shanghai Institute of Applied Physics, Chinese Academy of Sciences.

Acknowledgements

We thank Guangdong Zhong Ke Bao Biotechnology Co., Ltd for providing the workplace for natural seawater adsorption. We thank Prof. Liangbin Li from University of Science and Technology of China for his constructive suggestions. We thank Ms Yan Luo, Ms Rongrong Cui, Dr Hengti Wang and Mr Renduo Liu for their help in MS, and TEM analysis of the sample. We acknowledge support from the National Natural Science Foundation of China (grant number U1732151, 21676291, and U1832124), and Strategic Priority Research Program of the Chinese Academy of Sciences (XDA02030000).

Notes and references

1 OECD Nuclear energy agency and international atomic energy agency, 2016.
2 J. H. Zhu, Q. Liu, J. Y. Liu, R. R. Chen, H. S. Zhang, J. Yu, M. L. Zhang, R. M. Li and J. Wang, *ACS Appl. Mater. Interfaces*, 2018, **10**, 28877–28886.
3 M. Piechowicz, C. W. Abney, N. C. Thacker, J. C. Gilhula, Y. Wang, S. S. Veroneau, A. Hu and W. Lin, *ACS Appl. Mater. Interfaces*, 2017, **9**, 27894–27904.
4 C. Tsouris, *Nat. Energy*, 2017, **2**, 17022.
5 Y. Yuan, Y. J. Yang, X. J. Ma, Q. H. Meng, L. L. Wang, S. Zhao and G. S. Zhu, *Adv. Mater.*, 2018, **30**, 1706507.
6 S. Z. Kou, Z. G. Yang and F. Sun, *ACS Appl. Mater. Interfaces*, 2017, **9**, 2035–2039.
7 D. S. Sholl and R. P. Lively, *Nature*, 2016, **532**, 438.
8 M. Kanno, *J. Nucl. Sci. Technol.*, 1984, **21**, 1–9.
9 C. W. Abney, R. T. Mayes, T. Saito and S. Dai, *Chem. Rev.*, 2017, **117**, 13935–14013.
10 N. Seko, A. Katakai, S. Hasegawa, M. Tamada, N. Kasai, H. Takeda, T. Sugo and K. Saito, *Nucl. Technol.*, 2003, **144**, 274–278.
11 M. Tamada, In International Seminar On Nuclear War And Planetary Emergencies—42nd Session, 2010.
12 S. Das, S. Brown, R. T. Mayes, C. J. Janke, C. Tsouris, L. J. Kuo, G. Gill and S. Dai, *Chem. Eng. J.*, 2016, **298**, 125–135.
13 Y. Oyola, C. J. Janke and S. Dai, *Ind. Eng. Chem. Res.*, 2016, **55**, 4149–4160.
14 Y. Oyola and S. Dai, *Dalton Trans.*, 2016, **45**, 8824–8834.
15 S. Brown, Y. F. Yue, L. J. Kuo, N. Mehio, M. J. Li, G. Gill, C. Tsouris, R. T. Mayes, T. Saito and S. Dai, *Ind. Eng. Chem. Res.*, 2016, **55**, 4139–4148.
16 D. Wang, J. A. Song, J. Wen, Y. H. Yuan, Z. L. Liu, S. Lin, H. Y. Wang, H. L. Wang, S. L. Zhao, X. M. Zhao, M. H. Fang, M. Lei, B. Li, N. Wang, X. L. Wang and H. Wu, *Adv. Energy Mater.*, 2018, **8**, 1802607.
17 Y. Yuan, S. Zhao, J. Wen, D. Wang, X. Guo, L. Xu, X. Wang and N. Wang, *Adv. Funct. Mater.*, 2019, **29**, 1805380.
18 W. Luo, G. Xiao, F. Tian, J. J. Richardson, Y. Wang, J. Zhou, J. Guo, X. Liao and B. Shi, *Energy Environ. Sci.*, 2019, **12**, 607–614.
19 C. Liu, P. C. Hsu, J. Xie, J. Zhao, T. Wu, H. T. Wang, W. Liu, J. S. Zhang, S. Chu and Y. Cui, *Nat. Energy*, 2017, **2**, 17007.
20 Technology and applied R&D Needs for nuclear fuel resources, 2010, Nuclear Fuel Resources Workshop, Norwood, Massachusetts, USA, October 13–15, 2010.
21 J. Kim, C. Tsouris, Y. Oyola, C. J. Janke, R. T. Mayes, S. Dai, G. Gill, L. J. Kuo, J. Wood, K. Y. Choe, E. Schneider and H. Lindner, *Ind. Eng. Chem. Res.*, 2014, **53**, 6076–6083.
22 T. Saito, S. Brown, S. Chatterjee, J. Kim, C. Tsouris, R. T. Mayes, L. J. Kuo, G. Gill, Y. Oyola, C. J. Janke and S. Dai, *J. Mater. Chem. A*, 2014, **2**, 14674–14681.

23 S. Das, Y. Oyola, R. T. Mayes, C. J. Janke, L. J. Kuo, G. Gill, J. R. Wood and S. Dai, *Ind. Eng. Chem. Res.*, 2016, **55**, 4103–4109.
24 S. Das, Y. Oyola, R. T. Mayes, C. J. Janke, L. J. Kuo, G. Gill, J. R. Wood and S. Dai, *Ind. Eng. Chem. Res.*, 2016, **55**, 4110–4117.
25 Z. Xing, J. Hu, M. Wang, W. Zhang, S. Li, Q. Gao and G. Wu, *Sci. China: Chem.*, 2013, **56**, 1504–1509.
26 Y. C. Jean, J. D. Van Horn, W. S. Hung and K. R. Lee, *Macromolecules*, 2013, **46**, 8392.
27 J. Kansy, *Nucl. Instrum. Methods Phys. Res., Sect. A*, 1996, **374**, 235–244.
28 S. J. Tao, *J. Chem. Phys.*, 1972, **56**, 5499–5510.
29 H. Nakanishi, *International Symposium on Positron Annihilation Studies of Fluids*, 1988, pp. 292–298.
30 Y. Kobayashi, M. Yamawaki, T. Oka, S. Saiki, H. F. M. Mohamed, K. Hattori and Y. Watanabe, *Positron And Positronium Chemistry*, 2013, vol. 733, pp. 147–150.
31 Y. C. Jean and D. M. Schrader, *Positron and Positronium Chemistry*, Studies in Physical and Theoretical Chemistry, Elsevier, Amsterdam, 1988, vol. 607.
32 A. S. Ivanov, C. J. Leggett, B. F. Parker, Z. C. Zhang, J. Arnold, S. Dai, C. W. Abney, V. S. Bryantsev and L. F. Rao, *Nat. Commun.*, 2017, **8**, 1560.
33 A. P. Ladshaw, A. S. Ivanov, S. Das, V. S. Bryantsev, C. Tsouris and S. Yiacoumi, *ACS Appl. Mater. Interfaces*, 2018, **10**, 12580–12593.
34 C. W. Abney, R. T. Mayes, M. Piechowicz, Z. Lin, V. S. Bryantsev, G. M. Veith, S. Dai and W. Lin, *Energy Environ. Sci.*, 2016, **9**, 448–453.
35 S. Das, C. Tsouris, C. Zhang, J. Kim, S. Brown, Y. Oyola, C. J. Janke, R. T. Mayes, L. J. Kuo, J. R. Wood, G. A. Gill and S. Dai, *Ind. Eng. Chem. Res.*, 2016, **55**, 4294–4302.
36 V. S. Neti, S. Das, S. Brown, C. J. Janke, L. J. Kuo, G. A. Gill, S. Dai and R. T. Mayes, *Ind. Eng. Chem. Res.*, 2017, **56**, 10826–10832.
37 G. X. Tian, S. J. Teat, Z. Y. Zhang and L. F. Rao, *Dalton Trans.*, 2012, **41**, 11579–11586.
38 X. Q. Sun, C. Xu, G. X. Tian and L. F. Rao, *Dalton Trans.*, 2013, **42**, 14621–14627.
39 W. N. Zhang, B. Zheng, W. X. Shi, X. Y. Chen, Z. L. Xu, S. Z. Li, Y. R. Chi, Y. H. Yang, J. Lu, W. Huang and F. W. Huo, *Adv. Mater.*, 2018, **30**, 1800643.
40 B. F. Parker, Z. C. Zhang, C. J. Leggett, J. Arnold and L. F. Rao, *Dalton Trans.*, 2017, **46**, 11084–11096.
41 Q. Sun, B. Aguila, J. Perman, A. S. Ivanov, V. S. Bryantsev, L. D. Earl, C. W. Abney, L. Wojtas and S. Q. Ma, *Nat. Commun.*, 2018, **9**, 1644.
42 M. H. Sun, S. Z. Huang, L. H. Chen, Y. Li, X. Y. Yang, Z. Y. Yuan and B. L. Su, *Chem. Soc. Rev.*, 2016, **45**, 3479–3563.
43 N. Kabay and H. Egawa, *Sep. Sci. Technol.*, 1994, **29**, 135–150.
44 Uranium price, https://www.cameco.com/invest/markets/uranium-price, 2018.

